Nuclear Materials and Energy 46 (2026) 102065

Contents lists available at ScienceDirect

Nuclear Materials and Energy

journal homepage: www.elsevier.com/locate/nme

Modification of chemical and mechanical properties of p-W-O coating after Magnum-PSI D_2-N_2 plasma exposure and its consequences for the analysis of LIBS spectra

Indrek Jõgi [a,*], Peeter Paris [a], Kaarel Piip [a], Jordy Vernimmen [b], Beata Tyburska-Pueschel [b], Sven Lange [a], Taivo Jõgiaas [a], Matteo Passoni [c,d], David Dellasega [c,d], Gabriele Alberti [c], Hennie van der Meiden [b]

[a] Institute of Physics, University of Tartu, W. Ostwaldi str. 1, 50411 Tartu, Estonia
[b] DIFFER Dutch Institute for Fundamental Energy Research, De Zaale 20, 5612 AJ Eindhoven, the Netherlands
[c] Politecnico di Milano, Department of Energy, via Lambruschini 4a, 20156 Milano, Italy
[d] Institute for Plasma Science and Technology, CNR, via Cozzi 53, 20125 Milano, Italy

ARTICLE INFO

Keywords:
LIBS
Tungsten-oxide
Magnum-PSI
Plasma exposure
D retention

ABSTRACT

The present study investigated the effect of D_2-N_2 (7%) plasma exposure in Magnum-PSI on the D retention and chemical and mechanical properties of a porous W-O (p-W-O) coating. The variation of the chemical composition, crystalline phase and mechanical properties along the sample surface were determined by Nuclear Reaction Analysis (NRA), Rutherford Backscattering Spectroscopy (RBS), nanoindentation and Raman spectroscopy. These changes were compared to the Laser-Induced Breakdown Spectroscopy (LIBS) measurements. LIBS depth profiles of W and Mo were consistent with the profiles determined by NRA and RBS, showing a W-O layer, a thin W adhesion layer and a Mo substrate. Typically, the high D intensity was determined only during the first LIBS laser shot on a measurement spot, while the spatial distribution of D intensity determined by LIBS along the coating surface followed the D concentration determined by NRA. According to the Raman spectra, the investigated p-W-O coating corresponded to nanograins of W-O and the phase composition was relatively uniform along the coating surface. The elastic modulus of p-W-O coating was considerably lower than the modulus of Mo coating or bulk W coating and corresponded to the values found in other studies carried out with W-O mixtures. The elastic modulus of p-W-O coating decreased towards the edge of the coating. The study revealed that the modulus and the background intensity of the LIBS spectra had a negative correlation, suggesting that LIBS may be a suitable method for the estimation of the stiffness of tungsten co-deposits as a similar correlation is shown for other types of W coatings.

1. Introduction

Harnessing energy through the controlled fusion of light elements, such as hydrogen isotopes deuterium (D) and tritium (T) is a way towards sustainable and stable energy production. The most mature fusion technology based on tokamak reactors has seen tremendous progress in previous decades, but numerous technological issues still need to be addressed [1,2]. One such issue is the retention of radioactive T in the plasma-facing components (PFC) of the reactor's first wall and divertor [3–5]. In addition to finding methods for the reduction of the retention, it is necessary to quantify the amount of retained T in the reactor walls.

Laser-Induced Breakdown Spectroscopy (LIBS) is a method currently being studied for in-situ detection of hydrogen isotopes retention in the PFC [6,7]. The method uses short but powerful laser pulses to ablate and excite a small amount of material and the optical emission of the formed plasma plume is recorded by a spectrometer. The emission lines in the recorded spectrum correspond to the elements of the investigated material. In principle, LIBS can also determine the elemental depth profiles in the PFC by applying a number of laser shots into the same spot [5,7]. However, the quantitative determination of hydrogen isotope retention is not straightforward by LIBS due to uncertainties in the relationship between elemental concentration and emission line intensity as well as

* Corresponding author at: Institute of Physics, University of Tartu, W. Ostwaldi str. 1, 50411 Tartu, Estonia.
E-mail address: indrek.jogi@ut.ee (I. Jõgi).

https://doi.org/10.1016/j.nme.2026.102065
Received 11 October 2025; Received in revised form 22 December 2025; Accepted 15 January 2026
Available online 17 January 2026

often unknown laser ablation rates of different materials.

The intensities of LIBS emission lines and the ablation rates depend on the chemical and mechanical properties of the investigated material, known as matrix effects [8]. As a consequence, for quantified retention measurements, it is necessary to obtain LIBS results for different coatings that simulate the surface of PFCs. Some of these coatings resemble porous, nanocrystalline or compact W-O deposits, which will form in certain divertor regions from eroded W and O impurities inevitably present in plasma [9–11]. A predetermined amount of D can be added to these coatings during the deposition of the coating [5,12–18] or introduced by exposing the produced coatings to D_2 plasma, for example, using the linear plasma devices such as Magnum-PSI [19]. The content of the retained D is measured by an alternative method, such as Nuclear Reaction Analysis (NRA) [20]. LIBS applicability for the D retention measurement in different tungsten and tungsten-oxide coatings after D_2 plasma exposure by Magnum-PSI has been investigated in several previous studies [21–23]. The LIBS D line intensities were lower by an order of magnitude in the porous W-O coating than in the compact W coating which had comparable D concentration according to NRA measurements [22]. The laser ablation rates of these coatings also differed considerably [21–23].

The chemical composition, phase content, and mechanical properties of the already different as-deposited W-O coatings are further modified by the exposure to Magnum-PSI plasma [21,24]. The effect of plasma is non-uniform along the surface [21–23] and, therefore, the investigation of the composition and mechanical properties along the surface requires methods that allow good depth resolution (< 1 μm) and lateral resolution (< 1 mm). Chemical composition variation along the plasma-exposed surface can be measured using both the LIBS and NRA methods, which have sufficiently good resolution. One method that can be used to determine the variation in hardness and elastic modulus along the sample surface with good resolution is nanoindentation [25,26]. The hardness of the material influences the LIBS ablation rate and plasma plume properties, which in turn affect the elemental line intensities [27,28]. The high-resolution crystalline composition measurements can be made using micro-Raman spectroscopy. Recently, it has been demonstrated that Raman spectroscopy allows distinguishing between compact and porous W-O and W-N coatings, which are often used in hydrogen isotope retention studies [29].

The aim of the present study was to investigate the changes in the LIBS spectral features and depth profiles along the porous W-O surface exposed to Magnum-PSI plasma and connect these changes with the D concentration and other surface characteristics determined by nanoindentation and Raman spectroscopy.

2. Experiment

The porous W-O coating (p-W-O) was prepared using the pulsed laser deposition (PLD) method described in earlier studies [24]. The laser pulses were focused on a W target (purity 99.9%) and the ablated species expanded in a high-vacuum chamber (base pressure of 10^{-3} Pa), where an Ar gas with a pressure of 50 Pa was present [30]. The expanding species were collected on a grounded circular Mo substrate (diam. 30 mm) designed for the exposure to Magnum-PSI plasma. The substrate was 70 mm away from the target and at room temperature. The first layer consisted of 150 nm of dense nanocrystalline W that acted as an adhesion layer [21,22]. The adhesion layer was deposited in the same run as soon as the base pressure was reached. Then the Ar was introduced in the chamber and porous W was deposited [30,31]. According to Ion Beam Analysis (IBA) data, the thickness of p-W-O coating deposited on the adhesion layer was 0.93 ± 0.02 μm and it contained 50 at. % oxygen, due to subsequent oxidation in the open air, which is facilitated by the pores.

The p-W-O coating was exposed to Magnum-PSI D_2-7% N_2 plasma for 2400 s. During the plasma exposure, the magnetic field was kept at 0.8 T and the voltage of the target holder was −40 V. According to Thomson scattering measurements, the electron temperature varied between 1.05 and 1.3 eV and the electron density between 3×10^{19} and 4×10^{19} cm^{-3}. The ion flux was approximately 1.4×10^{23} D/m^2 and the corresponding fluence was 3.5×10^{26} D/m^2. The plasma beam had approximately a Gaussian shape with a Full Width at Half Maximum (FWHM) value of 19–22 mm. The surface temperature was kept at 380°C.

After the plasma exposure, the sample was moved to the Target Exchange and Analysis Chamber (TEAC) without breaking the vacuum. The LIBS measurements were carried out at a pressure of 1 mbar Ar within 1 to 1.5 h after the plasma exposure. A pulsed Nd:YAG laser (1064 nm, 8 ns) was used to produce the laser plasma plume. The fluence of the laser beam was 20 J/cm^2. The emission of the plasma plume was collected by a Czerny-Turner type spectrometer coupled with an iCCD camera. The delay time between the laser pulse and the collection of spectra was 1300 ns, and the gate width of the iCCD camera was 2000 ns. The spectral window was used around the 656 nm H_α line from 651 nm to 661 nm.

NRA and Rutherford Backscattering spectroscopy (RBS) measurements were carried out in the ion beam analysis station about 1 week after the plasma exposure. All samples were measured at 2000 keV using ^{3}He ion beam, which was perpendicular to the sample surface. The size of the beam was 1 mm × 1 mm and it was positioned approximately 2 mm away from a corresponding LIBS crater. The spectra were collected by the RBS ($\theta = 170°$, $\Omega = 0.874$ msr) and NRA ($\theta = 170°$, $\Omega = 9.423$ msr, 17×10^4 thin film units Kapton foil) detectors positioned at Cornell geometry. The collected charge is taken by fitting the RBS spectrum from pure tungsten and the NRA spectrum from the 275 nm a-C:D layer. The depth resolution, which determines the layer thickness, was calculated using RESOLNRA [32]. The depth profiles are calculated in thin film units (TFU), where 1 TFU = 10^{15} at/cm^2. The conversion from TFU to nm is made assuming pure dense tungsten. Therefore, the actual layer thickness in nm for oxidized, porous tungsten deviates from the calculated thickness. Independent of the type of substrate and oxide thickness, a maximum of 16,500 TFUs (= 2610 nm in pure W) was simulated in NRA spectra and a maximum of 8250 TFUs in RBS spectra. All spectra were simulated with SIMNRA [33].

Hardness and elastic modulus measurements were carried out using a Bruker Hysitron TI980 triboindenter. The measurements were made at 5 different locations along the coating surface, starting from the center of the sample and extending to the edge of the sample corresponding to the unexposed p-W-O coating. The locations are near the black dots as depicted in the rightmost picture in Fig. 1, and up to 30 measurements were made at each location (Fig. S1). In some cases, the number of measurements was smaller due to the technical setup of the indentation system. One reason being the creep in piezo-electric elements used for the positioning and, occasionally, thermal drift. This mostly influences first few measurements of a set and such measurements were omitted from the set. These influences can cause the measurement results to deviate 20% or even more compared to average results. The second reason was that some results were considerable outliers when compared to average results (Fig. S2, topmost result). The spacing between single measurements was 10 μm to avoid influence between the separate indents. Additional measurements were made from the backside of the sample to determine the hardness and elastic modulus of the Mo substrate. The hardness and elastic modulus were determined from the load–displacement curve of a nanoindentation test.[25] The hardness of the material is equal to the mean contact pressure, defined as the maximum force at the depth divided by the projected contact area at this depth. The elastic (Young's) modulus is calculated from the stiffness of the contact, determined from the derivative of the load and displacement of the unloading part of the curve [34]. The measurements were performed in continuous stiffness measurement mode, giving 60 separate data points at different depths in each measurement. The tip displacement started at 50–70 nm and ended at 600–750 nm. The starting and ending depths for a set are shown on Fig. S2. The calibration check after the initial calibration of the cube corner diamond tip is

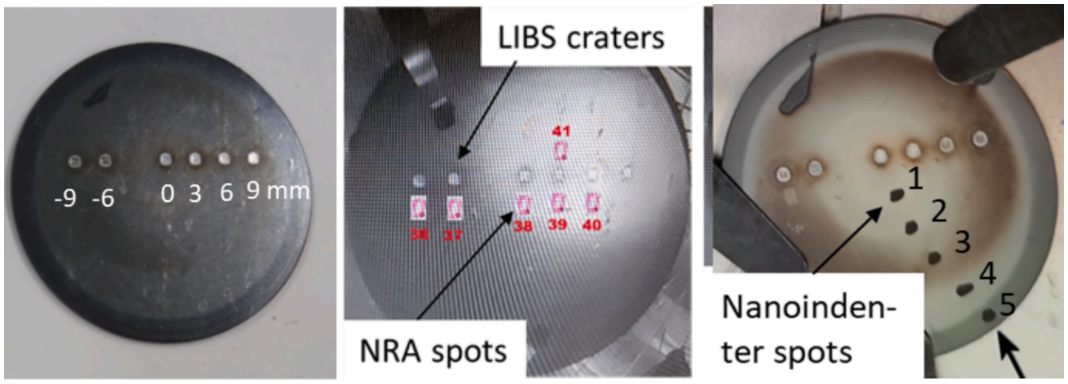

Fig. 1. The visual appearance of the coating after LIBS measurements and identification of the position of LIBS, NRA and black spots mark the positions next to the nanoindenter measurements.

shown in Fig. S3. Most measured points were within 70 ± 5 GPa in the displacement range of approximately 40 – 450 nm and the results should be mainly considered at that range. The fused quartz calibration sample has a defined reduced Young's modulus of 69.6 GPa, where the reduced modulus means that the calculations also considered the deformation of the tip [34]. Fig. S3 includes data from 8 different measurements.

Raman scattering measurements were carried out with a Renishaw inVia Raman micro-Raman setup using a solid-state laser working at 514 nm as the excitation source. The total laser power at our disposal was ≈10 mW. The power was attenuated 20x so that the estimated laser power at the sample was approximately 0.5 mW. The setup was equipped with an optical microscope and the objectives of the microscope were set at a 5x or 50x magnification. The latter allowed the lateral resolution of ~ 1 μm.

3. Results and Discussion

Fig. 1 (left) shows the image of the sample immediately after exposure to D_2-N_2 (7%) plasma and craters formed after the LIBS measurements. The photo in the middle of Fig. 1 was taken in the TEAC and shows the regions of NRA measurements in relation to LIBS craters. The Raman spectra were collected at similar positions at a distance of approximately 2 mm from the LIBS craters. The photo on the right of Fig. 1 shows the positions of nanoindenter measurements. In the last image of the sample, the central region of the plasma-exposed surface appeared lighter when compared to the outer regions. The appearance of darker or lighter areas has also been observed in several earlier studies [21,22]. It is a visual optical effect that characterizes the reflection properties of the surface and could be due to the changes in surface morphology. Changes in color could also be attributed to the changes in chemical composition or recrystallization.

3.1. LIBS measurements

Fig. 2 shows the spectra obtained from the crater at the lateral position of 0 mm (3rd spot from left in Fig. 1) for the first three laser shots and for the 12th laser shot. D_α and H_α line intensities at 656.1 and 656.28 nm, respectively, were weak and had signal to noise ratio in the range of 5 to 10. This is consistent with the earlier LIBS measurement results with a similar p-W-O coating [22]. The D_α line is clearly detectable during the first pulse, decreases abruptly during subsequent pulses and reaches the noise level after three pulses. In general, the D_α line was clearly missing during the 4th and 5th shots. The investigated spectral region featured W I lines at 653.23 and 657.39 nm and Mo I line at 651.97 nm [35]. W peaks were detectable in the recorded spectra during the first 5 laser shots and they were strongest during the 4th and 5th shots. Mo line started to appear from the 3rd shot and reached nearly constant value at 10–12 shots. Together with Mo I line, there appeared strong lines at 653.82, 654.46, 655.34, 655.62 and 655.86 nm which are missing from the databases [35,36]. We attribute these lines to Mo II. The background intensity of the spectrum was characteristically high during the first two to three laser shots, which ablated the porous

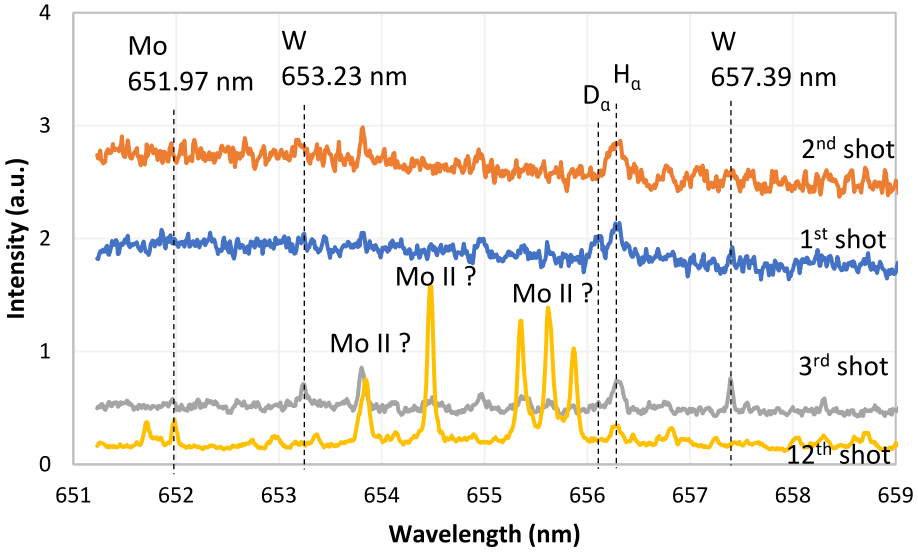

Fig. 2. LIBS spectra obtained from the LIBS crater at the lateral position of −6 mm for the first three laser shots and for the 12th laser shot.

coating. This observation is further discussed in relation to figure 5.

The intensities of W, Mo, D and H lines, which were used for the construction of elemental depth profiles, were obtained by fitting the peaks corresponding to metals with Gaussian line profile and lines of D_α and H_α with a Voigt profile (Fig. 3). The Voigt profile is a convolution of a Gaussian profile and a Lorentzian profile. The FWHM value of the Gaussian line profile used for fitting the metallic lines was 0.05 nm and it corresponded to the apparatus function of the spectrometer. The FWHM value of the Gaussian part of the Voigt profile, which was used in the fitting of D_α and H_α lines, considered both apparatus function and Doppler broadening. The FWHM value caused by Doppler broadening depends on the temperature of the plasma plume, which could not be determined in the present study due to the lack of suitable W lines. The FWHM value due to Doppler broadening, which varies from 0.036 to 0.05 nm for H_α and 0.025 nm to 0.036 for D_α when assuming electron temperature in the range of 0.5 to 1 eV. This temperature range is expected due to the relatively long delay time and low gas pressure used [37,38]. The FWHM value of Gaussian profile which also considered the apparatus function remained within 15% in the used temperature range. The FWHM value of a Lorentzian profile was used as a fitting parameter to obtain the best coincidence between the experimental and Voigt profiles. The FWHM value of the Lorentzian profile was 0.11 ± 0.03 nm for the first 3 laser shots and it decreased to 0.065 ± 0.005 nm for subsequent laser shots. In here, the uncertainty was mainly influenced by the fitting accuracy which was estimated by varying the FWHM value manually and estimating the upper and lower values which resulted in a reasonably good visual fit of the D_α and H_α peaks. The variability of FWHM values determined by using automatic fitting algorithm at different spots was approximately 20%. The Lorentzian line shape is the result of the Stark effect and the FWHM value of the line can be used to determine the electron density [39]. The FWHM values of 0.1 nm and 0.07 nm corresponded to the electron densities of approximately 9×10^{15} cm^{-3} and 4×10^{15} cm^{-3}, respectively.

LIBS depth profiles averaged over all six measurement spots on the sample surface (Fig. 4) show that Mo line originating from the substrate appeared after 3 shots and increased to a stable value after 10 shots. The number of laser shots required to reach half of this stable value was 6–7 and this value was used as the number of laser shots required to reach the Mo substrate. This method is used because the ablation in the center of the LIBS laser beam is larger than at the sides of the beam and therefore the number of laser shots required to reach the Mo substrate varies along the crater [40]. The W intensity was approximately two times higher at 4–5 laser shots when compared to the first three laser shots, and this depth is attributable to the 150 nm W interlayer as

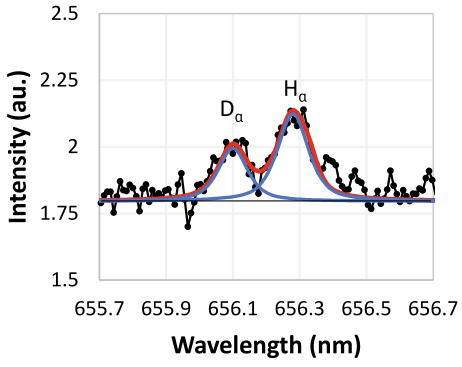

Fig. 3. Determination of D_α and H_α line intensities and background intensity by fitting the spectrum with Voigt profiles. The spectrum corresponds to the first laser shot at position −6 mm. Black circles show the experimental results, black line the background intensity, blue lines the theoretical D_α and H_α line intensities and red line the sum of the calculated line intensities. (For interpretation of the references to colour in this figure legend, the reader is referred to the web version of this article.)

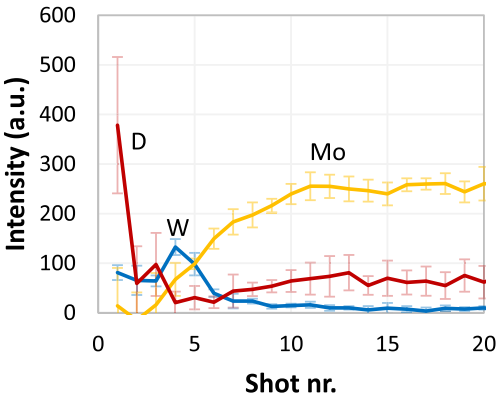

Fig. 4. LIBS depth profiles of p-W-O coating and 150 nm W interlayer on Mo substrate averaged over six measurement spots along the sample surface. LIBS depth profiles show the intensity as a function of laser shot number. The error bars show the standard deviation over the six measurement spots.

described in earlier studies [21,22]. The D_α line intensity was highest during the first laser shot and then decreased to the detection limit in the W interlayer. At higher laser shot numbers, a weak line at the position of the D_α line at 656.1 nm appeared again. This line may also correspond to other elements, such as a weak Mo line not listed in databases because it correlates with the Mo line intensity. Note that the O intensity is not shown in the depth profile because of the limited spectral range of the spectrometer.

The background intensity level in the wavelength region between 655.9 and 657.5 nm, below the D_α and H_α lines (shown in Fig. 3 by a black line) is shown as a function of the laser shot number in Fig. 5a. The background intensity was higher during the first three laser shots and then decreased to a low level when the dense W interlayer was reached. Such behavior of background intensity was also observed in earlier studies with p-W-O, c-W-O and c-W coatings [21,22] but was not previously reported. The average background intensity during the first three laser shots is shown in Fig. 5b as a function of position along the sample. The average intensity is somewhat lower in the central region of the sample, which appeared lighter in the photos. Increased background intensity can be the result of higher radiative recombination [41]. An alternative explanation could be the blackbody emission of droplets formed due to the ablation of nonevaporated porous material. In either case, the increased background emission intensity can be attributed to the porous W-O material with its higher ablation rate. It has been previously demonstrated that plasma exposure changes the crystal size, strain and hardness of tungsten, which has an impact on LIBS plasma plume properties and line intensities [27,28].

3.2. Comparison of LIBS and NRA measurements

The examples of LIBS depth profiles obtained at specific measurement spots are compared with the NRA/RBS depth profiles obtained at adjacent spots on the sample surface (Fig. 6). RBS depth profiles show approximately 950 nm thick W-O layer on a well-distinguished pure 150 nm thick W interlayer. The RBS measurements showed that the concentrations of O and W were approximately 50 at. % in the porous W-O layer. According to the NRA results, deuterium was mostly found in the 200–300 nm thick surface layer of W-O and the concentration of D varied between 0.8–3 at. % depending on the position along the sample surface. Somewhat lower D concentration, between 0.1–0.3 at. %, was detectable deeper in the p-W-O coating up to the W interlayer. NRA measurements did not detect D in the Mo substrate, which supports the assignment of the line at 656.1 nm observed at shot numbers above 10 to an unknown Mo line. The surface W-O layer with the highest D concentration contained slightly more W and less O with the difference of 7–9 at. % (Fig. 6d-f). One possible explanation for the lower O content at

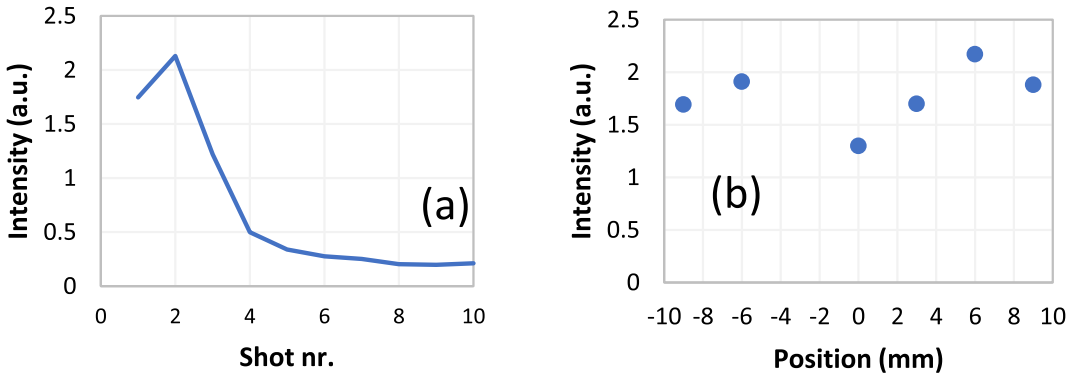

Fig. 5. Background intensity in the wavelength range of 655.9 to 657.5 nm around D_α and H_α lines in the region of 656 nm (a) as a function of laser shot number for the crater at 3 mm and (b) average value over the first three shots as a function of position along the sample surface.

the coating surface is the reduction of O during the exposure to D plasma [42].

In general, LIBS depth profiles corresponded reasonably well to the NRA/RBS depth profiles but were less accurate. Unlike previous LIBS studies, which investigated similar plasma-exposed coatings [21,22], the W lines were relatively strong allowing for a clear distinction between the p-W-O layer and the W interlayer. The average laser ablation rate of the p-W-O layer was estimated by dividing the coating thickness determined by RBS by the number of laser shots required to reach the W interlayer. This number was between 3 and 4. The corresponding ablation rate was 220 to 310 nm/shot for p-W-O. The number of laser shots required to ablate the dense W interlayer was between 1 and 2 and the corresponding ablation rate was 70 to 150 nm/shot. These values are consistent with the ablation rates of similar coatings determined in previous studies [21,22].

The observed highest D_α line intensity value during the first laser shot is consistent with the highest D concentrations in the 200–300 nm surface layer according to NRA, assuming an ablation rate of 200–250 nm per shot. The peak value of D_α line was approximately 5–10 times larger than the standard deviation of the background noise at wavelength range 652.07 to 652.30 nm where lines were missing. The D concentration at the surface varied from 0.8 to 3.0 at. %. The resulting LOD value was approximately 0.5 at. % for the used LIBS parameters.

The D concentration in the topmost p-W-O layer with a higher D percentage determined by NRA is shown in Fig. 7 as a function of position along the sample surface together with the D/W line ratio determined by LIBS. The line ratio was calculated with the D intensity of the first laser shot and the W intensities averaged over the first 5 shots. This approach was chosen because the W line intensities during the first laser shot were not sufficiently strong to be used for normalization. The W intensity value over 5 shots is a measure of total W in the layers and the averaging over 5 shots allows to improve the signal-to-noise ratio. The NRA and LIBS results are generally consistent along the sample surface and show an increase in D concentration from one side to the other. This could be the result of asymmetric cooling of the sample due to the asymmetric clamping on the sample holder. There was no clear correlation with the visual appearance of the sample surface. It must be noted that at single position (6 mm), LIBS results deviated from the trend. However, considerable variation in D intensities has also been observed in our previous study [23]. It may be related to the uneven distribution of D on the surface, as also observed in a study by PIXE [43]. The concentrations determined by NRA (0.8–2.5 at. %) were of the same order of magnitude but somewhat larger than in our previous study (0.2–1.5 at. %), where p-W-O coating was exposed to D_2 plasma at similar conditions (plasma parameters, fluence and surface temperature) [22]. According to previous studies [44], the D retention is expected to increase when the tungsten coatings are exposed to nitrogen-containing plasma. However, previous studies were conducted with metallic tungsten and thorough studies with p-W-O coatings are still lacking.

3.3. Surface hardness and elastic modulus measurements

The hardness and elastic modulus as a function of indenter tip displacement are shown in Fig. 8 for the p-W-O coating at position 1 and for the Mo substrate. There were up to 30 measurements at each location (Fig. S1 in the Appendix). The average hardness of bulk Mo was 2.7 GPa, which is comparable to the value found in another study [45]. The hardness of Mo at depths of 50–100 nm varied considerably, from 5 to 10 GPa. Similarly, the hardness of the p-W-O at the surface varied from 10 to 17 GPa, while the value at a depth of 400–500 nm was approximately 7 GPa. The average value of the elastic modulus of Mo was 285 GPa, close to the value of the expected bulk modulus of 320 GPa [46]. The elastic modulus of p-W-O coating varied from 115 to 150 GPa depending on the position on the surface and was about two times smaller than the modulus of bulk Mo or different W materials used in fusion applications [47]. The measured elastic modulus values were comparable with the elastic modulus of approximately 150 GPa determined for similar WO coatings by Surface Brillouin Spectroscopy [11]. For sputtered W-O compounds, it has been shown that the hardness and Young's modulus depend strongly on the O/W ratio and reduced to 7 GPa and 150 GPa respectively for WO_2 and WO_3 [48,49]. Previous studies have also shown that higher porosity results in lower hardness and modulus [50,51].

The increase in the value of the elastic modulus with increasing tip displacement can be related to the material pile-up near the tip during the indentation (Fig. S4 in the Appendix). Pile-up increases the contact area and volume between the material and the diamond tip, thereby increasing the force required for deformation, which in turn results in higher moduli values [52,53]. The local features present in the indentation area are also important and are a likely reason for the variation of hardness and moduli at different positions. The modulus and hardness are lower when indenter tip is placed at a higher surface where the mechanical contact area is smaller and critical mechanical stress for plastic deformation is achieved at lower forces. The reverse situation, where the tip is between surface features, results in the measurement of higher modulus and hardness [54]. The effect of roughness is especially important at low values of indentation displacements. In addition to the effect of surface roughness, the non-uniform material structure related to the porosity could also influence the results. For instance, if the contact area or material density changes, it will lead to a different condition regarding the deformation and indentation in general. The density change can occur when the pores collapse under applied load, or the pore walls are crushed. Due to the effect of the described factors, the accurate description of plastic deformation mechanics is very difficult to give for the porous samples.

For comparison of the moduli at different distances from the sample

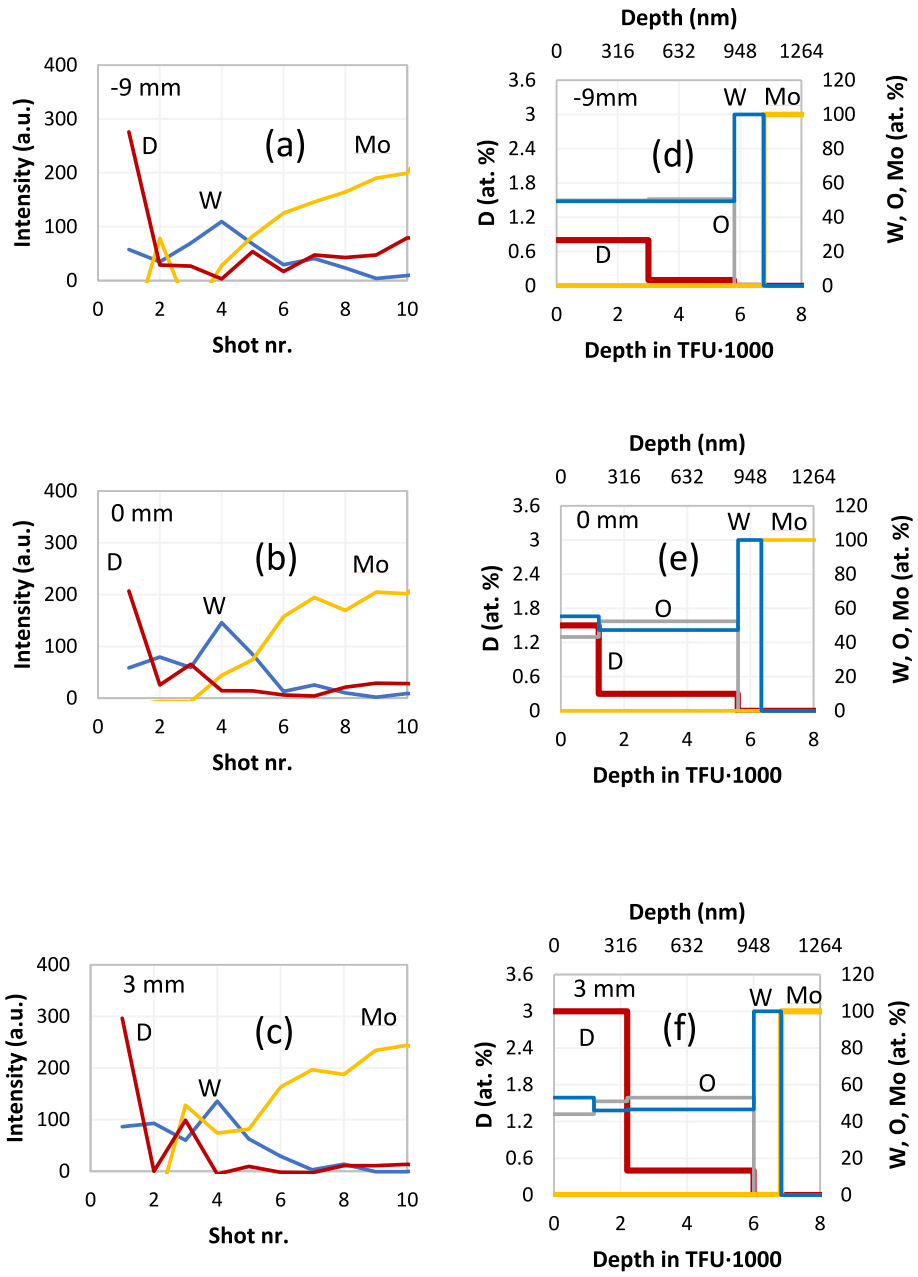

Fig. 6. LIBS (a-c) and NRA/RBS (d-f) depth profiles of p-W-O coating and 150 nm W interlayer on Mo substrate determined at three positions along the sample surface. LIBS depth profiles show the intensity as a function of laser shot number, while NRA/RBS depth profiles show the atomic concentrations as a function of TFU (Thin Film Units with 10^{15} at/cm^2) and depth in nm corresponding to the stoichiometric W-O layer. The red lines show D, blue lines W, grey lines O and yellow lines Mo. (For interpretation of the references to colour in this figure legend, the reader is referred to the web version of this article.)

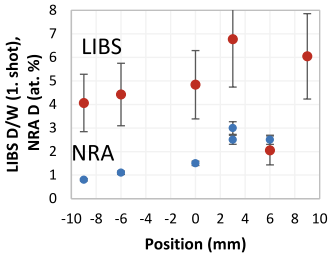

Fig. 7. LIBS D/W ratio and NRA D in at. % at different positions along the sample surface (positions shown in Fig. 1).

center, measurements near a specific position were averaged over all results and at a comparable tip displacement. Fig. 9a shows the results for different locations along the coating surface and the value for the Mo substrate. The modulus of the p-W-O coating somewhat increased towards the center of the sample. The average hardness at the depth of 100 nm also increased from 7 to 11 GPa towards the center of the sample, but still this effect was within the significant variation of the hardness values (Fig. 8a). Deuterium plasma exposure has been shown to result in tungsten embrittlement by increasing hardness and reducing the elastic modulus [26,55]. The growth of the elastic modulus in the central region suggests that the plasma exposure also caused the densification of the porous W-O surface. The increased material hardness and modulus after ion implantation have also been observed in other studies [56,57].

A negative correlation occurred between LIBS background intensity

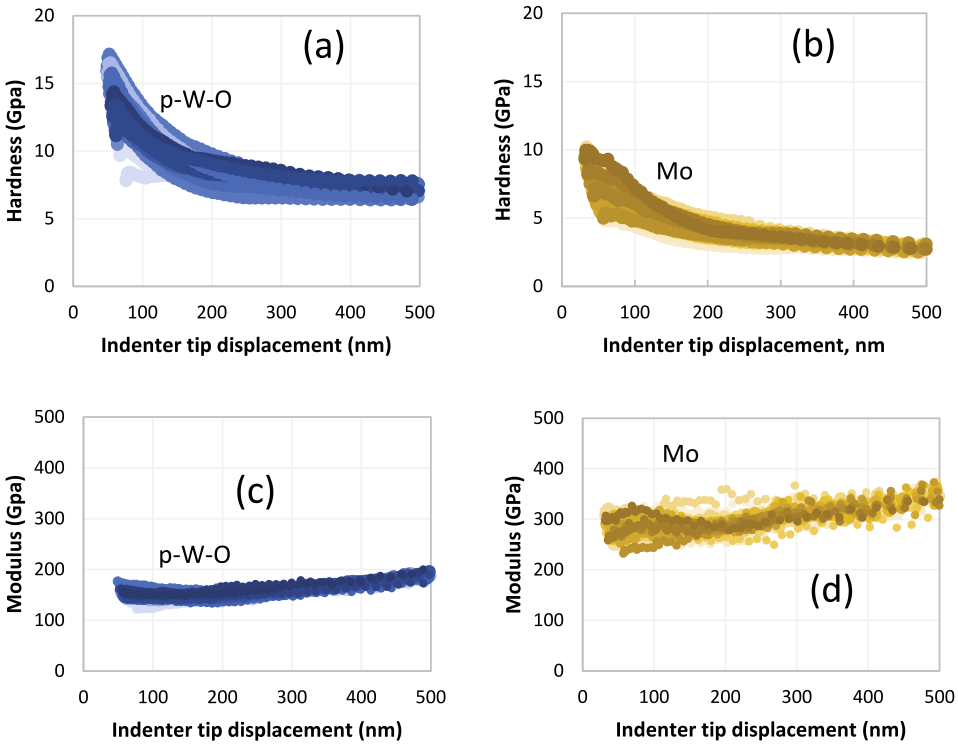

Fig. 8. Hardness (a,b) and elastic modulus (c,d) as a function of tip displacement for (a,c) p-W-O coating at position 1 and (b,d) Mo substrate. The graphs show the results of 26 (p-W-O) and 29 (Mo) different measurements.

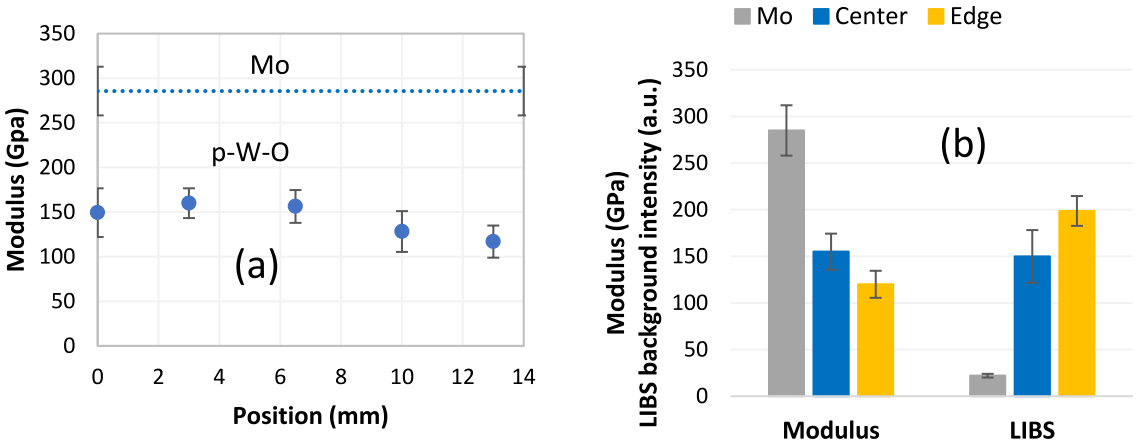

Fig. 9. (a) The average modulus at different positions along the p-W-O surface and on the Mo substrate. The position at 0 mm corresponds to the center of the sample. (b) The comparison of the modulus and the LIBS background intensity of p-W-O coating in the center and edge of the sample and Mo.

and modulus. The LIBS background intensity was an order of magnitude higher in p-W-O when compared to the Mo substrate (Fig. 9b). At the same time, the modulus was approximately two times lower in p-W-O. The LIBS background intensity of p-W-O coating slightly increased towards the edge of the coating, while the modulus was lower. Therefore, the LIBS background intensity correlates inversely with the stiffness of the material. It is necessary to carry out more systematic studies with various types of coatings to assess the importance of this effect and determine the causal relationship between the background intensity and the mechanical strength of the material. Previous studies have shown porous materials have lower hardness and modulus [(43,44)]. Porous materials also have higher ablation rates, as is also apparent in the present study. This, in turn, may result in higher background intensity.

3.4. Raman measurements

Raman spectroscopy was used to determine the phase composition of the coating and to investigate whether the phase composition of the p-W-O coating surface is homogeneous over the entire coating surface or influenced by plasma exposure. Fig. 10a shows Raman spectra obtained at the outer region of the coating. In these measurements, a magnification of 5 was used to collect data over a larger area. At the same time, the laser intensity was kept low (0.5 mW) to avoid phase changes in the W-O coating [29]. Due to the low signal strength, 100 spectra were accumulated with the acquisition time of 30 s per spot. Registered spectra are similar to the results of other measurements of c-W-O coatings prepared by PLD and correspond to amorphous or nanocrystalline tungsten oxides [29,58,59]. The spectrum exhibits broad bands at 200–400 cm^{-1}, 530 cm^{-1}, 800 cm^{-1} and 930 cm^{-1}. The most dominant

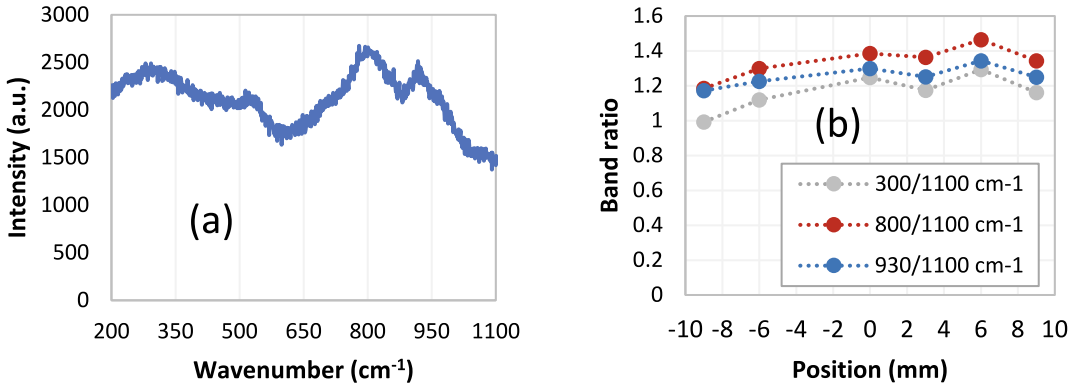

Fig. 10. (a) Raman spectra registered from the p-W-O coating at 6 mm. (b) The ratio of the intensity of bands at 300, 800 and 930 cm^{-1} with the intensity at 1100 cm^{-1} as a function of position.

feature at 800 cm^{-1} is attributable to WO_3 nanocrystals and the feature at 930 cm^{-1} could be attributed to the W=O mode at the grain boundaries. The higher intensity of this band suggests a larger surface area of nanograins [29,58–60]. The nanograin size in similar p-W-O coatings has been < 10 nm [30,61]. The broad feature at 530 cm^{-1} may be due to the formation of WN during the D_2-N_2 plasma exposure [29]. The spectra obtained at the central and edge regions of the sample were similar. The intensities of the bands at 300, 800 and 930 cm^{-1} were divided by the intensity at 1100 cm^{-1} to compare the peaks obtained at different positions. The ratios are shown in Fig. 9b. The ratio was somewhat higher in the center and on one side of the sample, but the variation was smaller than that of the D concentration.

Raman measurements may result in recrystallization during the measurements when the laser intensity is sufficiently high [29]. At a magnification of 50x and high laser intensities (full available power 10 mW at the time of the experiment), lines corresponding to WO_3 crystallites (260, 720 and 810 cm^{-1}) appeared. The sample surface darkened in the spot where Raman measurements were made. This ensures that the first series of measurements was carried out at sufficiently low intensities to prevent considerable recrystallization during the Raman measurements.

An additional question was the micro-scale uniformity of the crystalline composition. Therefore, mapping of a small region of the surface was performed at medium laser intensity and magnification of 50x (Fig. 11). The size of each measurement spot was 1 μm. There appeared to be certain spots where the darkening of the surface occurred. In these spots, the Raman spectra contained features corresponding to WO_3 (upper spectrum in Fig. 11). The spectra collected from the rest of the investigated area remained almost featureless, corresponding to the spectrum of porous W-O. The WO_3 formed preferentially in spots that were already darker in the microscope image taken before Raman measurements (Fig. 11). This suggests that certain regions were already crystallized to WO_3 or were more prone to recrystallization due to laser heating. Such microscopic variation may be related to the variation of D retention as observed previously in plasma-exposed tungsten coatings by micro-NRA [43].

4. Conclusions

LIBS depth profiles of the investigated p-W-O coating are consistent with depth profiles determined by ion beam analysis methods. Notably, the LIBS depth profile reveals clearly visible compact W adhesion layer between the p-W-O coating and Mo substrate, which is consistent with RBS and previous SEM measurements of the coating cross-sections. The depth resolution of LIBS measurements remained inferior to that of IBA measurements. However, this can be improved by using top-hat laser beams and optimizing laser fluence.

The LIBS intensity of D peak remained weak even when D concentration exceeded 1 at. % according to NRA measurements with the LOD value of approximately 0.5 at. %. Reasonably strong D intensity was

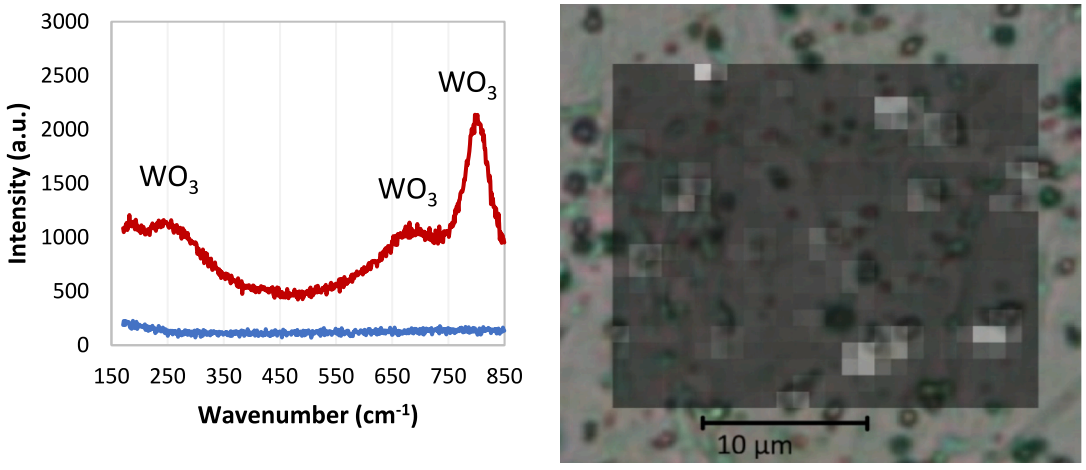

Fig. 11. Raman spectra registered at different regions of the map correspond either to WO_3 (red line) or porous W-O (blue line). Lighter rectangles on the map correspond to the spots where Raman spectra had a higher intensity of the WO_3 band at 810 cm^{-1}. The map showing the intensity of the WO_3 peak is superimposed on the photo of the investigated region with the common scalebar. For easier comparison, the map is somewhat smaller than the photo and is generally darker. Lighter squared spots correspond to the higher WO_3 band in the Raman spectrum. (For interpretation of the references to colour in this figure legend, the reader is referred to the web version of this article.)

determined only during the first laser shot of a measurement spot. The result is consistent with earlier studies, which have demonstrated that for dense W and columnar W-O coatings with similar D concentration, the LIBS D intensity is an order of magnitude higher. The lateral distribution of LIBS D intensity in the coating followed the D percentage determined by NRA. The D intensity varied approximately 2 times in different regions of the coating, as determined by both NRA and LIBS. There was no clear correlation with the visual appearance of the sample surface, but the variation of D concentration along the surface could be due to the asymmetric temperature profile along the sample.

The elastic modulus of p-W-O coating was approximately two times lower than that of Mo coating. In addition, the modulus and hardness decreased towards the edge of the sample. This suggests that the plasma exposure densifies the surface of the coating. The modulus had a negative correlation with the LIBS background intensity, which suggests that the latter could be used to estimate the elastic modulus and stiffness of the coating. More comprehensive studies with various types of tungsten coatings are required to clarify this result. Additionally, the fundamental causes of the increased background intensity need to be analyzed. Since the ablation is also influenced by the hardness of the material, the results can lead to a method for the determination of the ablation rate from LIBS spectra.

Raman spectra confirmed the presence of porous W-O, which was consistent with the expected properties of the investigated coating. The Raman spectra obtained along the coating surface with smaller magnification were generally similar along the sample surface, suggesting the phase composition of the p-W-O coating surface is not strongly affected by the spatial variation of the plasma beam. The microscopic differences on the surface were revealed when larger magnification and higher intensity were used. Most of the surface had spectra corresponding to very defective W-O nanocrystals, while certain spots could have some WO_3 crystallites.

CRediT authorship contribution statement

Indrek Jõgi: Writing – review & editing, Writing – original draft, Visualization, Investigation, Formal analysis. **Peeter Paris:** Writing – review & editing, Supervision, Methodology, Conceptualization. **Kaarel Piip:** Methodology, Conceptualization. **Jordy Vernimmen:** Writing – review & editing, Methodology, Investigation, Data curation. **Beata Tyburska-Pueschel:** Writing – review & editing, Methodology, Investigation, Formal analysis. **Sven Lange:** Writing – review & editing, Methodology, Investigation. **Taivo Jõgiaas:** Writing – review & editing, Methodology, Investigation, Formal analysis, Data curation. **Matteo Passoni:** Writing – review & editing, Resources. **David Dellasega:** Writing – review & editing, Resources. **Gabriele Alberti:** Resources. **Hennie van der Meiden:** Writing – review & editing, Supervision, Project administration, Methodology, Investigation, Funding acquisition, Conceptualization.

Declaration of competing interest

The authors declare that they have no known competing financial interests or personal relationships that could have appeared to influence the work reported in this paper.

Acknowledgements

This work has been carried out within the framework of the EUROfusion Consortium, funded by the European Union via the Euratom Research and Training Programme (Grant Agreement No 101052200—EUROfusion). Views and opinions expressed are however those of the author(s) only and do not necessarily reflect those of the European Union or the European Commission. Neither the European Union nor the European Commission can be held responsible for them.

Appendix A. Supplementary data

Supplementary data to this article can be found online at https://doi.org/10.1016/j.nme.2026.102065.

Data availability

Data will be made available on request.

References

[1] C. Windsor, Can the development of fusion energy be accelerated? an introduction to the proceedings, Philosophical transactions of the Royal Society a: Mathematical, Phys. Eng. Sci. 377 (2019), https://doi.org/10.1098/rsta.2017.0446.

[2] G. Federici, P. Andrew, P. Barabaschi, J. Brooks, R. Doerner, A. Geier, A. Herrmann, G. Janeschitz, K. Krieger, A. Kukushkin, A. Loarte, R. Neu, G. Saibene, M. Shimada, G. Strohmayer, M. Sugihara, Key ITER plasma edge and plasma-material interaction issues, J. Nucl. Mater. 313–316 (2003) 11–22, https://doi.org/10.1016/S0022-3115(02)01327-2.

[3] J.P. Girard, P. Garin, N. Taylor, J. Uzan-Elbez, L. Rodríguez-Rodrigo, W. Gulden, ITER, safety and licensing, Fusion Eng. Des. 82 (2007) 506–510, https://doi.org/10.1016/j.fusengdes.2007.03.017.

[4] M. Lukacs, L.G. Williams, Nuclear safety issues for fusion power plants, Fusion Eng. Des. 150 (2020) 111377, https://doi.org/10.1016/j.fusengdes.2019.111377.

[5] A. Malaquias, V. Philipps, A. Huber, A. Hakola, J. Likonen, J. Kolehmainen, S. Tervakangas, M. Aints, P. Paris, M. Laan, A. Lissovski, S. Almaviva, L. Caneve, F. Colao, G. Maddaluno, M. Kubkowska, P. Gasior, H.J. Van Der Meiden, A.R. Lof, P.A. Zeijlmans Van Emmichoven, P. Petersson, M. Rubel, E. Fortuna, Q. Xiao, Development of ITER relevant laser techniques for deposited layer characterisation and tritium inventory, J. Nucl. Mater. 438 (2013) S936–S939, https://doi.org/10.1016/j.jnucmat.2013.01.203.

[6] V. Philipps, A. Malaquias, A. Hakola, J. Karhunen, G. Maddaluno, S. Almaviva, L. Caneve, F. Colao, E. Fortuna, P. Gasior, M. Kubkowska, A. Czarnecka, M. Laan, A. Lissovski, P. Paris, H.J. van der Meiden, P. Petersson, M. Rubel, A. Huber, M. Zlobinski, B. Schweer, N. Gierse, Q. Xiao, G. Sergienko, Development of laser-based techniques for in situ characterization of the first wall in ITER and future fusion devices, Nucl. Fusion 53 (2013) 093002, https://doi.org/10.1088/0029-5515/53/9/093002.

[7] H.J. Van Der Meiden, S. Almaviva, J. Butikova, V. Dwivedi, P. Gasior, W. Gromelski, A. Hakola, X. Jiang, I. Jõgi, J. Karhunen, M. Kubkowska, M. Laan, G. Maddaluno, A. Marín-Roldán, P. Paris, K. Piip, M. Pisarčík, G. Sergienko, M. Veis, P. Veis, S. Brezinsek, Monitoring of tritium and impurities in the first wall of fusion devices using a LIBS based diagnostic, Nucl. Fusion 61 (2021) 125001, https://doi.org/10.1088/1741-4326/ac31d6.

[8] B.C. Windom, D.W. Hahn, Laser ablation - Laser induced breakdown spectroscopy (LA-LIBS): a means for overcoming matrix effects leading to improved analyte response, J. Anal. At. Spectrom 24 (2009) 1665–1675, https://doi.org/10.1039/b913495f.

[9] A. Litnovsky, M. Matveeva, A. Herrmann, V. Rohde, M. Mayer, K. Sugiyama, K. Krieger, V. Voitsenya, G. Vayakis, A.E. Costley, R. Reichle, G. De Temmerman, S. Richter, U. Breuer, L. Buzi, S. Möller, V. Philipps, U. Samm, P. Wienhold, First studies of ITER-diagnostic mirrors in a tokamak with an all-metal interior: results of the first mirror test in ASDEX Upgrade, Nucl. Fusion 53 (2013), https://doi.org/10.1088/0029-5515/53/7/073033.

[10] M. Rasinski, E. Fortuna-Zalesna, M. Mayer, R. Neu, T. Plocinski, M. Lewandowska, K.J. Kurzydlowski, High resolution scanning transmission electron microscopy (HR STEM) analysis of re-deposited layer on ASDEX Upgrade tile, Fusion Eng. Des. 86 (2011) 1753–1756, https://doi.org/10.1016/j.fusengdes.2011.02.085.

[11] E. Besozzi, D. Dellasega, A. Pezzoli, C. Conti, M. Passoni, M.G. Beghi, Amorphous, ultra-nano- and nano-crystalline tungsten-based coatings grown by Pulsed Laser Deposition: Mechanical characterization by Surface Brillouin Spectroscopy, Mater. Des. 106 (2016) 14–21, https://doi.org/10.1016/j.matdes.2016.04.096.

[12] S. Almaviva, L. Caneve, F. Colao, R. Fantoni, G. Maddaluno, Remote-LIBS characterization of ITER-like plasma facing materials, J. Nucl. Mater. 421 (2012) 73–79, https://doi.org/10.1016/j.jnucmat.2011.11.050.

[13] S. Almaviva, L. Caneve, F. Colao, G. Maddaluno, N. Krawczyk, A. Czarnecka, P. Gasior, M. Kubkowska, M. Lepek, Measurements of deuterium retention and surface elemental composition with double pulse laser induced breakdown spectroscopy, Phys. Scr. 2016 (2016) 014043, https://doi.org/10.1088/0031-8949/T167/1/014043.

[14] P. Paris, J. Butikova, M. Laan, M. Aints, A. Hakola, K. Piip, I. Tufail, P. Veis, Detection of deuterium retention by LIBS at different background pressures, Phys. Scr. T170 (2017) 014003.

[15] M. Suchonova, P. Veis, J. Karhunen, P. Paris, M. Pribula, K. Piip, M. Laan, C. Porosnicu, C. Lungu, A. Hakola, Determination of deuterium depth profiles in fusion-relevant wall materials by nanosecond LIBS, Nucl. Mater. Energy 12 (2017) 611–616.

[16] P. Paris, J. Butikova, M. Laan, A. Hakola, I. Jõgi, J. Likonen, E. Grigore, C. Ruset, Comparison of LIBS results on ITER-relevant samples obtained by nanosecond and picosecond lasers, Nucl. Mater. Energy 18 (2019), https://doi.org/10.1016/j.nme.2018.11.018.

[17] P. Veis, A. Marin-Roldan, V. Dwivedi, J. Karhunen, P. Paris, I. Jõgi, C. Porosnicu, C. P. Lungu, V. Nemanic, A. Hakola, Quantification of H/D content in Be/W mixtures coatings by CF-LIBS, Phys. Scr. T171 (2020) 014073.
[18] V. Dwivedi, M. Veis, A. Marín Roldán, E. Grigore, F. Baiasu, I. Bogdanovič Radovič, Z. Siketić, P. Veis, CF-LIBS study of pure Ta, and WTa + D coating as fusion-relevant materials: a step towards future in situ compositional quantification at atmospheric pressure, Eur Phys J plus 136 (2021) 1177, https://doi.org/10.1140/epjp/s13360-021-02179-0.
[19] M.J. van de Pol, S. Alonso van der Westen, D.U.B. Aussems, M.A. van den Berg, S. Brons, H.J.N. van Eck, G.G. van Eden, H.J.W. Genuit, H.J. van der Meiden, T. W. Morgan, J. Scholten, J.W.M. Vernimmen, E.G.P. Vos, M.R. de Baar, Operational characteristics of the superconducting high flux plasma generator Magnum-PSI, Fusion Eng. Des. 136 (2018) 597–601, https://doi.org/10.1016/j.fusengdes.2018.03.033.
[20] P. Wang, W. Jacob, L. Gao, T. Dürbeck, T. Schwarz-Selinger, Comparing deuterium retention in tungsten films measured by temperature programmed desorption and nuclear reaction analysis, Nucl Instrum Methods Phys Res B 300 (2013) 54–61, https://doi.org/10.1016/j.nimb.2013.01.057.
[21] I. Jõgi, P. Paris, M. Laan, J. Kozlova, H. Mändar, M. Passoni, D. Dellasega, A. Hakola, H.J. van der Meiden, LIBS study of ITER relevant tungsten–oxygen coatings exposed to deuterium plasma in Magnum-PSI, J. Nucl. Mater. 544 (2021) 152660, https://doi.org/10.1016/j.jnucmat.2020.152660.
[22] P. Paris, I. Jõgi, K. Piip, M. Passoni, D. Dellasega, E. Grigore, W.M. Arnoldbik, H. van der Meiden, In-situ LIBS and NRA deuterium retention study in porous W-O and compact W coatings loaded by Magnum-PSI, Fusion Eng. Des. 168 (2021) 23–27, https://doi.org/10.1016/j.fusengdes.2021.112403.
[23] I. Jõgi, P. Paris, K. Piip, J. Ristkok, R. Talviste, H.M. Piirsoo, A. Tamm, E. Grigore, A. Hakola, B. Tyburska-Pueschel, H.J. van der Meiden, LIBS applicability for investigation of re-deposition and fuel retention in tungsten coatings exposed to pure and nitrogen-mixed deuterium plasmas of Magnum-PSI, Phys. Scr. 96 (2021) 114010, https://doi.org/10.1088/1402-4896/ac169c.
[24] A. Pezzoli, D. Dellasega, V. Russo, A. Gallo, P.A.Z. Zeijlmans van Emmichoven, M. Passoni, E. Besozzi, D. Dellasega, V. Russo, C. Conti, M. Passoni, M.G. Beghi, A. Maffini, A. Uccello, D. Dellasega, M. Passoni, Thermal annealing and exposure to divertor-like deuterium plasma of tailored tungsten oxide coatings, J. Nucl. Mater. 463 (2015) 1041–1044, https://doi.org/10.1016/j.matdes.2018.107565.
[25] M. Spychalski, E. Fortuna-Zalesna, J. Zdunek, M. Rubel, A. Widdowson, S. Aleiferis, B. Thomas, Tungsten Langmuir probes from JET-with the ITER-Like Wall: Assessment of mechanical properties by nano-indentation, Phys. Scr. 96 (2021) 124072, https://doi.org/10.1088/1402-4896/ac3dbb.
[26] X. Fang, A. Kreter, M. Rasinski, C. Kirchlechner, S. Brinckmann, C. Linsmeier, G. Dehm, Hydrogen embrittlement of tungsten induced by deuterium plasma: Insights from nanoindentation tests, J. Mater. Res. 33 (2018) 3530–3536, https://doi.org/10.1557/jmr.2018.305.
[27] H. Sattar, H. Ran, W. Ding, M. Imran, M. Amir, H. Ding, An approach of stand-off measuring hardness of tungsten heavy alloys using LIBS, Appl. Phys. B 126 (2020) 1–11, https://doi.org/10.1007/s00340-019-7355-0.
[28] H. Sattar, S. Jielin, H. Ran, M. Imran, W. Ding, P. Das Gupta, H. Ding, Impact of microstructural properties on hardness of tungsten heavy alloy evaluated by stand-off LIBS after PSI plasma irradiation, Journal of Nuclear Materials 540 (2020) 152389, https://doi.org/10.1016/j.jnucmat.2020.152389.
[29] C. Pardanaud, D. Dellasega, M. Passoni, C. Martin, P. Roubin, Y. Addab, C. Arnas, L. Couëdel, M. Minissale, E. Salomon, G. Giacometti, A. Merlen, E. Bernard, R. Mateus, E. Alves, Z. Siketic, I.B. Radovic, A. Hakola, Post-mortem analysis of tungsten plasma facing components in tokamaks: Raman microscopy measurements on compact, porous oxide and nitride films and nanoparticles, Nucl. Fusion 60 (2020) 086004, https://doi.org/10.1088/1741-4326/ab9347.
[30] D. Dellasega, G. Merlo, C. Conti, C.E. Bottani, M. Passoni, Nanostructured and amorphous-like tungsten films grown by pulsed laser deposition, J. Appl. Phys. 112 (2012) 084328, https://doi.org/10.1063/1.4761842.
[31] R. Mateus, D. Dellasega, M. Passoni, Z. Siketić, I. Bogdanović Radović, J. Likonen, A. Hakola, E. Alves, Deuterium loading of redeposited-like W coatings present in tokamaks by ion implantation, Vacuum 227 (2024) 113403, https://doi.org/10.1016/j.vacuum.2024.113403.
[32] M. Mayer, RESOLNRA: a new program for optimizing the achievable depth resolution of ion beam analysis methods, Nucl Instrum Methods Phys Res B 266 (2008) 1852–1857, https://doi.org/10.1016/j.nimb.2007.11.071.
[33] M. Mayer, SIMNRA User's Guide, in: Technical Report UPP 9/113, Max-Planck -Institute Für Plasmaphysik, Garching, 1997.
[34] W.C. Oliver, G.M. Pharr, Measurement of hardness and elastic modulus by instrumented indentation: advances in understanding and refinements to methodology, J. Mater. Res. 19 (2004) 3–20.
[35] and N.A.T. Kramida, A., Ralchenko, Yu., Reader, J., NIST Atomic Spectra Database (ver. 5.6.1), [Online], Https://Physics.Nist.Gov/Asd [2019, September 5]. National Institute of Standards and Technology, Gaithersburg, MD. (2019).
[36] R.L. Kurucz, B. Bell, Atomic Line Data, Kurucz CD-ROM No.23, Smithsonian Astrophysical Observatory, Cambridge, Mass, 1995.
[37] A. Lissovski, K. Piip, L. Hämarik, M. Aints, M. Laan, P. Paris, A. Hakola, J. Karhunen, LIBS for tungsten diagnostics in vacuum: selection of analytes, J. Nucl. Mater. 463 (2015) 923–926, https://doi.org/10.1016/j.jnucmat.2014.11.096.
[38] I. Jõgi, P. Paris, E. Bernard, M. Diez, E. Tsitrone, A. Hakola, J. Likonen, T. Vuoriheimo, E. Grigore, Ex Situ LIBS Analysis of WEST Divertor Wall Tiles after C3 Campaign, Journal of Nuclear, Engineering 4 (2023) 96–110, https://doi.org/10.3390/jne4010007.
[39] M.A. Gigosos, M.A. Gonzalez, V. Cadenoso, Computer simulated Balmer-alpha, -beta and -gamma Stark line profiles for non-equilibrium plasma diagnostics, Spectrochim Acta Part B At, Spectrosc 58 (2003) 1489–1504, https://doi.org/10.1016/S0584-8547.
[40] G. Shaw, M. Bannister, T.M. Biewer, M.Z. Martin, F. Meyer, B.D. Wirth, The detection of He in tungsten following ion implantation by laser-induced breakdown spectroscopy, Appl. Surf. Sci. 427 (2018) 695–703, https://doi.org/10.1016/j.apsusc.2017.08.180.
[41] A. De Giacomo, R. Gaudiuso, M. Dell'Aglio, A. Santagata, The role of continuum radiation in laser induced plasma spectroscopy, Spectrochim Acta Part B At, Spectrosc 65 (2010) 385–394, https://doi.org/10.1016/j.sab.2010.03.016.
[42] D. Dellasega, G. Alberti, E. Fortuna-Zalesna, W. Zielinski, A. Pezzoli, S. Möller, B. Unterberg, M. Passoni, A. Hakola, Nanostructure formation and D retention in redeposited-like W exposed to linear plasmas, Nucl. Mater. Energy 36 (2023), https://doi.org/10.1016/j.nme.2023.101492.
[43] M. Kelemen, A. Založnik, P. Vavpetič, M. Pečovnik, P. Pelicon, A. Hakola, A. Lahtinen, J. Karhunen, K. Piip, P. Paris, M. Laan, K. Krieger, M. Oberkofler, H. van der Meiden, S. Markelj, Micro-NRA and micro-3HIXE with 3He microbeam on samples exposed in ASDEX Upgrade and Pilot-PSI machines, Nucl Instrum Methods Phys Res B 404 (2017) 179–184, https://doi.org/10.1016/j.nimb.2017.01.072.
[44] A. Kreter, D. Nishijima, R.P. Doerner, M. Freisinger, C. Linsmeier, Y. Martynova, S. Möller, M. Rasinski, M. Reinhart, A. Terra, Y. Torikai, B. Unterberg, Influence of plasma impurities on the fuel retention in tungsten, Nucl. Fusion 59 (2019), https://doi.org/10.1088/1741-4326/ab235d.
[45] L. Zhang, X. Zhang, N. Li, P. Zhang, X. Mei, Y. Wang, V.V. Uglov, Experimental and simulation studies on damage mechanisms of tungsten and molybdenum under compressed plasma flow irradiation, Nucl. Fusion 63 (2023) 076010, https://doi.org/10.1088/1741-4326/acd016.
[46] K.H. Matucha, R.W. Cahn, P. Haasen, E.J. Kramer, Materials Science and Technology: A comprehensive Treatment, Vol. 8, Structure and Properties of Nonferrous Alloys, 1996.
[47] S. Krimpalis, K. Mergia, S. Messoloras, A. Dubinko, D. Terentyev, K. Triantou, J. Reiser, G. Pintsuk, Comparative study of the mechanical properties of different tungsten materials for fusion applications, Phys. Scr. 2017 (2017), https://doi.org/10.1088/1402-4896/aa9292.
[48] N.M.G. Parreira, N.J.M. Carvalho, A. Cavaleiro, Synthesis, structural and mechanical characterization of sputtered tungsten oxide coatings, Thin Solid Films 510 (2006) 191–196, https://doi.org/10.1016/j.tsf.2005.12.299.
[49] I. Moirangthem, S.H. Chen, B.S. Lou, J.W. Lee, Microstructural, mechanical and optical properties of tungsten oxide coatings fabricated using superimposed HiPIMS-MF systems, Surf. Coat. Technol. 436 (2022), https://doi.org/10.1016/j.surfcoat.2022.128314.
[50] X. Chen, Y. Xiang, J.J. Vlassak, Novel technique for measuring the mechanical properties of porous materials by nanoindentation, J. Mater. Res. 21 (2006) 715–724, https://doi.org/10.1557/jmr.2006.0088.
[51] Z. Chen, X. Wang, V. Bhakhri, F. Giuliani, A. Atkinson, Nanoindentation of porous bulk and thin films of La0.6Sr 0.4Co0.2Fe0.8O3-δ, Acta Mater. 61 (2013) 5720–5734, https://doi.org/10.1016/j.actamat.2013.06.016.
[52] F.B. Kværndrup, C. Engelbrekt, Ö.C. Kücükyildiz, M.A.J. Somers, T.L. Christiansen, G. Winther, Area determination with pile-up and sink-in in nanoindentation of oxygen containing titanium, Mater. Today Commun. 30 (2022), https://doi.org/10.1016/j.mtcomm.2022.103218.
[53] Y. Xia, M. Bigerelle, J. Marteau, P.E. Mazeran, S. Bouvier, A. Iost, Effect of surface roughness in the determination of the mechanical properties of material using nanoindentation test, Scanning 36 (2014) 134–149, https://doi.org/10.1002/sca.21111.
[54] M. Kull, H.M. Piirsoo, A. Tarre, H. Mändar, A. Tamm, T. Jõgiaas, Hardness, Modulus, and Refractive Index of Plasma-Assisted Atomic-Layer-Deposited Hafnium Oxide Thin Films Doped with Aluminum Oxide, Nanomaterials 13 (2023), https://doi.org/10.3390/nano13101607.
[55] W.Q. Chen, X.Z. Xiao, B. Pang, S.S. Si, Y.Z. Jia, B. Xu, T.W. Morgan, W. Liu, Y. L. Chiu, Irradiation hardening induced by blistering in tungsten due to low-energy high flux hydrogen plasma exposure, J. Nucl. Mater. 522 (2019) 11–18, https://doi.org/10.1016/j.jnucmat.2019.05.004.
[56] A. Shypylenko, A.V. Pshyk, B. Grześkowiak, K. Medjanik, B. Peplinska, K. Oyoshi, A. Pogrebnjak, S. Jurga, E. Coy, Effect of ion implantation on the physical and mechanical properties of Ti-Si-N multifunctional coatings for biomedical applications, Mater. Des. 110 (2016) 821–829, https://doi.org/10.1016/j.matdes.2016.08.050.
[57] X. Xie, C. Chen, J. Luo, J. Xu, Effect of Nitrogen Ion Implantation Energy on the Mechanical and Chemical Properties of AISI M50 Steel, Int. J. Chem. Eng. 2021 (2021), https://doi.org/10.1155/2021/4630661.
[58] F. Di Fonzo, A. Bailini, V. Russo, A. Baserga, D. Cattaneo, M.G. Beghi, P.M. Ossi, C. S. Casari, A. Li Bassi, C.E. Bottani, Synthesis and characterization of tungsten and tungsten oxide nanostructured films, Catal Today 116 (2006) 69–73, https://doi.org/10.1016/j.cattod.2006.02.080.
[59] A. Baserga, V. Russo, F. Di Fonzo, A. Bailini, D. Cattaneo, C.S. Casari, A. Li Bassi, C. E. Bottani, Nanostructured tungsten oxide with controlled properties, Synthesis

and Raman Characterization, Thin Solid Films 515 (2007) 6465–6469, https://doi.org/10.1016/j.tsf.2006.11.067.

[60] M. Boulova, G. Lucazeau, Crystallite Nanosize effect on the Structural Transitions of WO3 Studied by Raman Spectroscopy, J. Solid State Chem. 167 (2002) 425–434, https://doi.org/10.1006/jssc.2002.9649.

[61] R. Mateus, D. Dellasega, M. Passoni, Z. Siketić, I. Bogdanović Radović, A. Hakola, E. Alves, Helium load on W-O coatings grown by pulsed laser deposition, Surf Coat Technol 355 (2018) 215–221, https://doi.org/10.1016/j.surfcoat.2018.02.089.